PHILOSOPHICAL TRANSACTIONS OF THE ROYAL SOCIETY A MATHEMATICAL, PHYSICAL & ENGINEERING SCIENCES

Fluidization, segregation and stress propagation in granular materials

J. M. Huntley

Phil. Trans. R. Soc. Lond. A 1998 **356**, 2569-2590
doi: 10.1098/rsta.1998.0287

THE ROYAL SOCIETY

Fluidization, segregation and stress propagation in granular materials

By J. M. Huntley

Loughborough University, Department of Mechanical Engineering, Loughborough LE11 3TU, UK

Results from recent experimental investigations into the fluidization, size-segregation and stress-transmission behaviour of model granular materials are described. Digital high-speed photography and particle-tracking software are used to study the vibro-fluidization of a two-dimensional powder. The dependence of granular temperature on vibration frequency, amplitude and number of grains is compared with simulations and a simple analytical model. Particle tracking at low base accelerations has also shown that a single large intruder in a two-dimensional bed of monodisperse particles moves upwards at the same speed as the smaller grains over a wide range of accelerations, suggesting that convection is the key to size segregation under these conditions. Force profiles have been measured under conical sandpiles by using a simple elasto-optical technique, which provides a spatial resolution comparable to the grain diameter. The results confirm the existence of counter-intuitive pressure dips at the centre of the pile. Simple two-dimensional models for force transmission in granular materials are reviewed; these are extended to three dimensions and to lattices with perturbations induced by deformation of the grains or by polydispersity.

Keywords: contact-force measurement; granular temperature; sandpiles; convection; high-speed photography; vibrated bed

1. Introduction

A significant body of literature has emerged recently on the physics of granular materials (see, for example, Jaeger & Nagel 1992). The response to vertical vibration, in particular, has been studied extensively. A wide range of unusual phenomena is observed (Evesque 1992), including heaping and convection rolls (Evesque & Rajchenbach 1989), and size segregation (Knight *et al*. 1993; Duran *et al*. 1993, 1994). At larger vibration amplitudes, period-doubling instabilities can lead to wave formation on the free surface (Douady *et al*. 1989; Pak & Behringer 1993), and eventually the system may become fully fluidized. The transmission of stress within a granular material may also produce counter-intuitive results, leading, for example, to a local minimum in the normal component of stress under the peak of a conical pile of sand (Smid & Novosad 1981). This paper reviews some of the research carried out into these areas by the author and co-investigators over the past four years.

2. Fluidization

Previous experimental studies of two-dimensional systems have generally considered the case of surface fluidization, whereby a condensed phase and fluidized phase coexist (Clement & Rajchenbach 1991). Full fluidization in one and two dimensions has

been investigated numerically by molecular dynamics and event-driven simulation techniques. Luding *et al*. (1994*a*, *b*) obtained the conditions required to observe the condensed and fluidized regimes and found empirical scaling relations for the height of the centre of mass for the system of grains. Fluidization behaviour can also be modelled by using kinetic theories of rapid granular flow. The reviews by Campbell (1990) and Savage (1984), on computer simulations and theory, respectively, discuss the concept of granular temperature and its relevance to granular materials. For the results presented here, we define granular temperature E_0 as the mean kinetic energy of a particle measured in the centre-of-mass frame, i.e.

$$E_0 = \tfrac{1}{2}m\overline{c^2}, \tag{2.1}$$

where m is the mass and c is the speed of the grain.

(*a*) *Instrumentation*

The fluidization and segregation experiments were carried out by using an electromagnetically driven shaker. The moving part of the shaker is a platform 156 mm in diameter which can attain a maximum peak-to-peak displacement under sinusoidal excitation of 25.4 mm, and a maximum velocity and acceleration of 1.06 m s^{-1} and $70g$ ($g = 9.81$ m s^{-2}), respectively. A cell made up of two glass plates, 165 mm wide by 285 mm high, was mounted on the moving platform. The plate separation was controlled by spacers; by adjusting the plate spacing to exceed the particle diameter by 0.05 mm, a close approximation to an idealized two-dimensional model powder was obtained. Vertical accelerations were monitored by using piezoelectric accelerometers, and displacements of the vibrating cell were measured by using a calibrated laser-displacement meter.

A Kodak Ektapro 1000 high-speed video camera system was used to record the two-dimensional motion of the particles, with the resulting images stored digitally on memory boards within the camera. Up to 1600 full-size images of 239×192 pixels can be recorded at a framing rate of up to 1000 frames per second, giving a total of 1.6 s of recording time. Images are transferred by GPIB interface to a Sun IPX SPARCstation, where the in-plane coordinates of particle centres are located by using image processing software. There are three steps to the image analysis.

1. The edges of the particles are detected by means of a Sobel filter.
2. The positions of the centres are calculated by Hough transformation of the resulting image.
3. The positions of all the detected particles within the field of view are tracked from frame to frame, from which velocity distribution functions can be calculated.

These procedures are described in detail by Warr *et al*. (1994).

(*b*) *Two-dimensional results*

The instrumentation described in § 2 *a* was used to investigate the fluidization of two-dimensional model powders consisting of 5 mm diameter steel spheres (Warr *et al*. 1995). One-dimensional powders have also been studied, both experimentally and

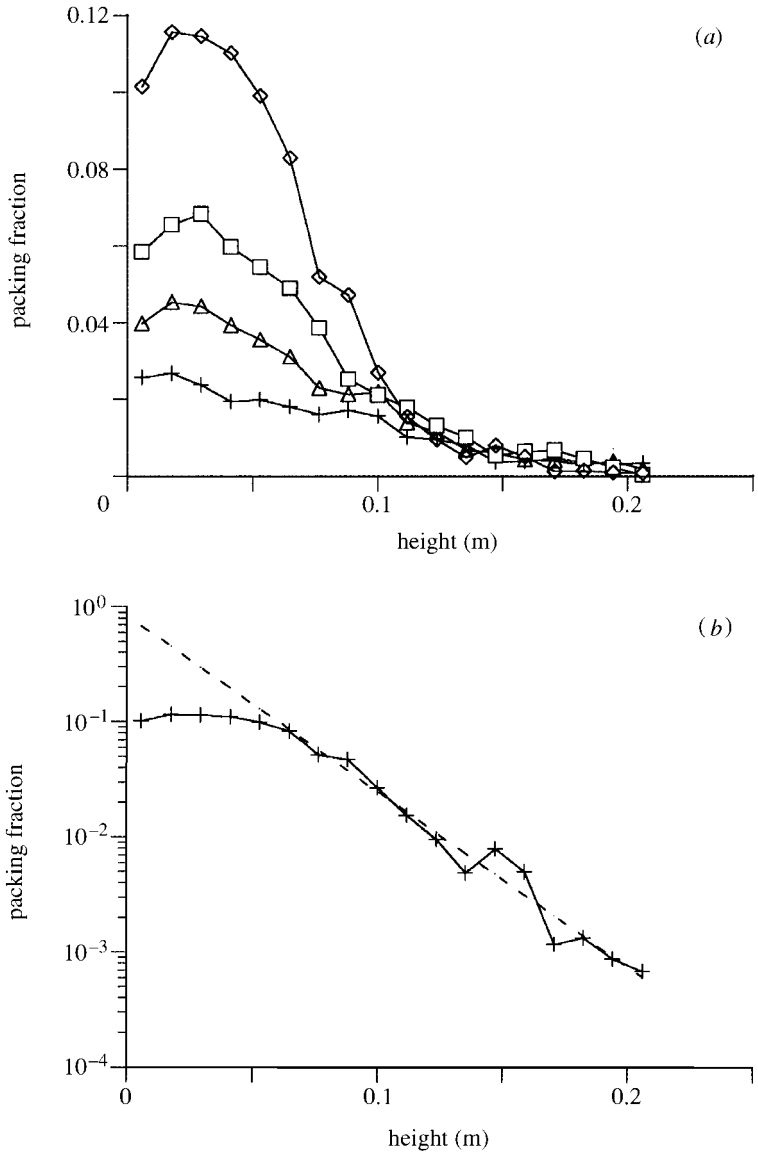

Figure 1. Effect of system size on the average packing fraction profiles. (*a*) Crosses, triangles, squares and diamonds correspond to $N = 27$, 40, 60 and 90, respectively; (*b*) $N = 90$ data with best-fit Boltzmann distribution.

theoretically (Warr & Huntley 1995; Warr *et al*. 1996), but only the two-dimensional results will be described here. The number of spheres in the cell, N, took the values 27, 40, 60 and 90, and for each of these, experiments were carried out with vibration amplitudes A_0 of 0.5, 1.123, 1.84 and 2.12 mm. The base frequency was 50 Hz throughout. One high-speed sequence was recorded at three different heights for each of these combinations of N and A_0, resulting in a total of nearly 80 000 frames of data.

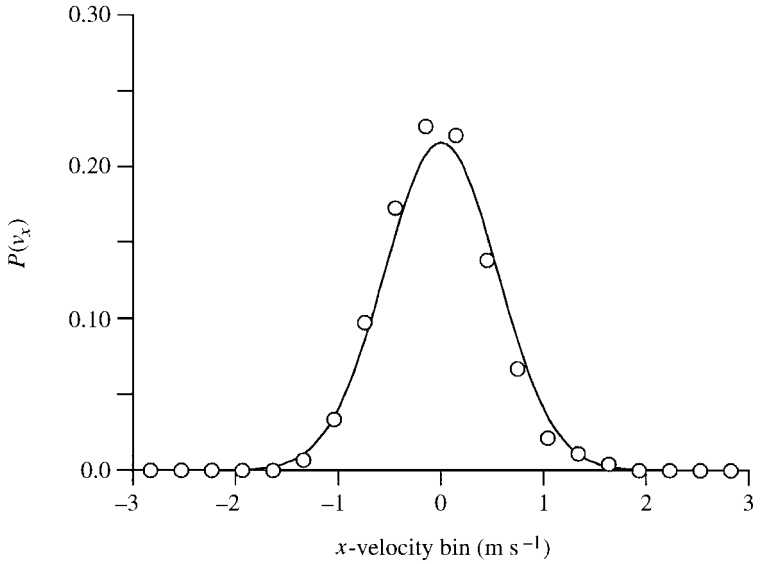

Figure 2. Horizontal velocity distribution: experimental (discrete points) with best-fit Gaussian.

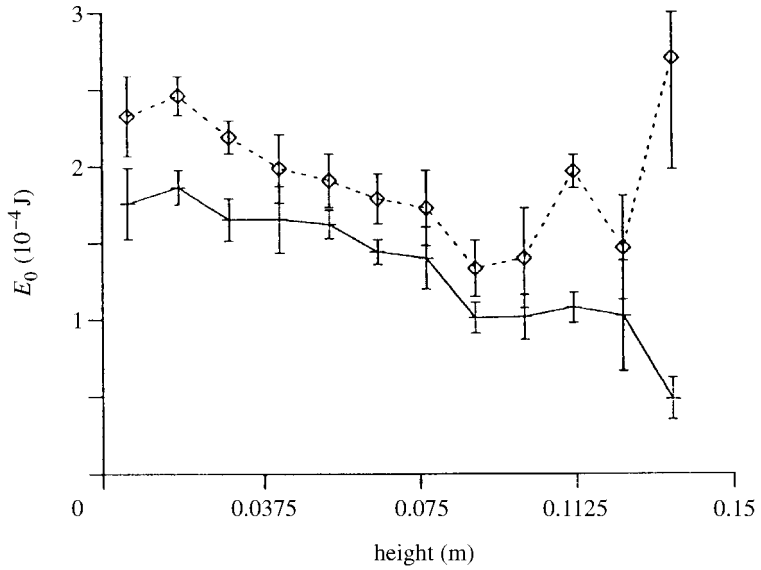

Figure 3. Horizontal and vertical granular temperature profiles from Gaussian fits to velocity distributions ($A_0 = 2.12$ mm, $N = 90$). Crosses and diamonds correspond to the x and y components of the granular temperature, respectively.

The measured packing fraction for all four N-values at $A_0 = 2.12$ mm, averaged across the width of the cell, are shown in figure 1*a*. The data for $N = 90$ are replotted on log-linear axes in figure 1*b*, together with a linear fit to the exponential tail of the distribution. The gradient of the best-fit line provides one measure of the

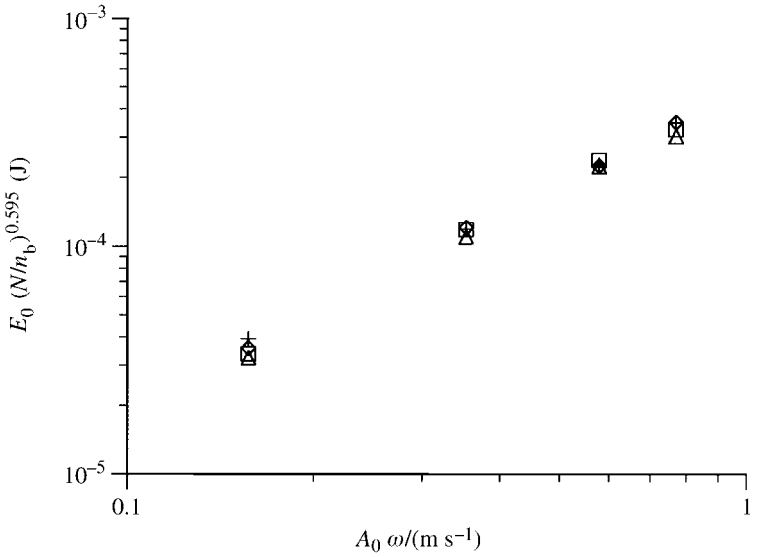

Figure 4. Granular temperature as a function of peak base velocity.

granular temperature, E_0. E_0 can also be estimated directly from the width of the measured velocity distribution functions. Figure 2 shows the distribution for the horizontal component of velocity at a height in the cell of 65 mm, where $N = 90$ and $A_0 = 2.12$ mm. Circles correspond to data points, and the line is the best-fit Gaussian curve. This method allows the spatial variation of E_0 within the cell to be mapped out. Figure 3 shows the results from the experiment with $N = 90$ and $A_0 = 2.12$ mm. The vertical component of temperature is higher than the horizontal, because energy is supplied through vertical motion of the cell. There is a general decrease in temperature with height, except possibly for an increase at the free surface.

Luding *et al.* (1994*a*, *b*) proposed the following scaling relationship between E_0 and A_0 and N, based on their simulation results:

$$E_0 \propto (A_0\omega)^{\alpha}[N(1-\varepsilon)]^{-\beta}, \tag{2.2}$$

where ω is the angular frequency of the base and ε is the restitution coefficient. The exponents α and β were found by Luding *et al.* (1994*a*, *b*) to take the values 2.0 and 1.0, respectively, for a one-dimensional powder, and the values 1.5 and 1.0 in two dimensions. An α value differing from 2 implies that the mean particle speed does not scale linearly with the mean speed of the vibrating base. Figure 4 shows the variation of E_0 with $A_0\omega$ as calculated from the speed (rather than from vertical or horizontal velocity) distribution functions. N has been normalized by n_b (the cell width divided by the grain diameter), and the effects of system size have been scaled out by using the average exponent $\beta = 0.60$. The data points fall on a line with a gradient $\alpha = 1.41 \pm 0.03$. A third method of calculating E_0 is from the height of the centre of mass of the fluidized material; all three methods resulted in α values in the range 1.3–1.4 and β values between 0.3 and 0.6.

(c) Two-dimensional model

Warr *et al*. (1995) proposed a simple model for a low-density vibro-fluidized granular material undergoing almost-elastic collisions. The granular temperature was assumed to be constant throughout the material; from the resulting Boltzmann distribution of particle density, the rate of energy dissipation could be calculated. The value of E_0 set up under steady-state conditions for a given excitation could then be obtained by equating this to the rate of energy input from the base. Warr *et al*. (1995) assumed the mean free path between collisions, λ, took the standard value from two-dimensional gas-kinetic theory,

$$\lambda = \frac{1}{2nd}, \tag{2.3}$$

where n is the number density and d is the grain diameter. This resulted in predicted α and β values of 2 and 1, respectively; both were therefore significantly higher than the experimental and simulation values. At high packing densities, however, the mean free path, λ_{h}, may differ from equation (2.3) because the particles are no longer randomly distributed. Each grain is surrounded by, on average, six nearest neighbours, whose relative positions become progressively more correlated as the density increases. In effect, the nearest neighbours act as a cage, the size of which defines λ_{h}:

$$\lambda_{\mathrm{h}} = \frac{B}{n^{1/2}}, \tag{2.4}$$

where B is a numerical constant of order unity (Helal *et al*. 1997). The different dependence on n and d for the two mean free paths results in differing scaling laws for the granular temperature. In particular, E_0 is predicted to scale as $(A_0\omega)^{4/3}$ and as $N^{-1/3}$, in closer agreement with the experimental results (Huntley 1998*a*). When the number of grains per unit length of cell is increased significantly above the values used in these experiments, the validity of the assumption of a constant granular temperature becomes questionable. Helal *et al*. (1997) suggested a model which involves solving two coupled differential equations for the packing fraction and granular temperature. There is good qualitative agreement with the experimental results and with molecular dynamics simulations (including the unexpected rise in granular temperature at the free surface). Currently, the main barrier to the effective use of such an approach is the difficulty in specifying the boundary conditions (packing fraction, temperature and temperature gradient) at the base of the cell.

3. Size segregation

The segregation of vibrated powders according to particle size is a well-known phenomenon, and can cause significant problems during handling. Several microscopic mechanisms have been presented in the literature. In the low-amplitude and high-frequency regime, convection rolls, driven by particle-wall friction, control segregation (Knight *et al*. 1993). The large grains are seen to be carried upwards at the same velocity as the small ones, leading to a continuous ascent. At very low accelerations, recent experiments on two-dimensional systems have identified a transition from a continuous to an intermittent, step-like, motion as the ratio of large to small particle sizes, Φ, decreases below a critical ratio (Duran *et al*. 1994). The experiments have

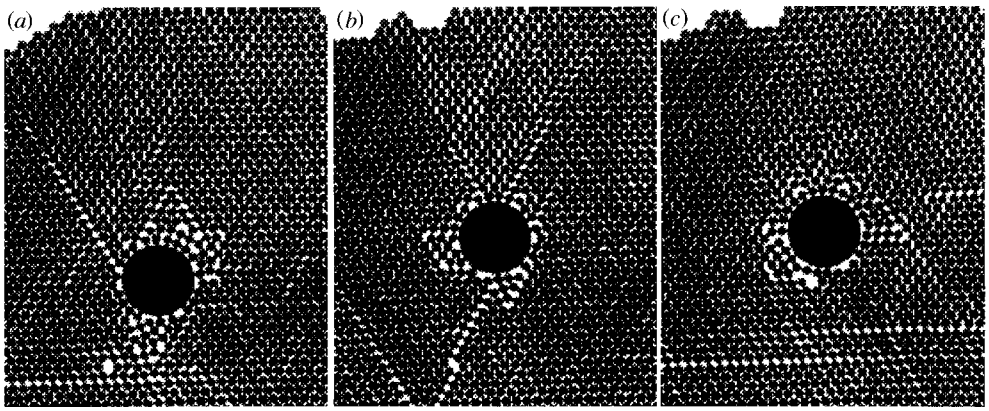

Figure 5. Images from size segregation experiments (see text for details).

indicated that segregation in this regime is no longer driven by convection, with the larger particles rising relative to the background particles. An arching-effect model has been proposed (Duran *et al*. 1993) to explain this transition.

The ability to measure and track particles with the Ektapro camera has been used to investigate the transition between the continuous and intermittent regimes (Cooke *et al*. 1996). The experiments were carried out by using a monolayer of approximately 5000 oxidized duralumin spheres (diameter of 2 mm) in the test cell, together with a single large 'intruder' particle. The intruders were 1 mm thick duralumin discs supported by three 2 mm diameter chrome steel sphere spacers. The spacers were pushed into 2 mm diameter holes drilled near the circumference of the intruder at 120° intervals. Γ is used to denote the peak acceleration normalized by g, the acceleration due to gravity. The vibration frequency throughout was 10 Hz.

Figure 5 shows three frames of an intruder with $\Phi = 7$, taken from the low-acceleration, $\Gamma = 1.17$, regime. Regions of disorder often appear around the intruder (figure 5*a*). Small gaps may open up below, into which particles can be pushed by collective block motion. Large gaps and avalanche events are not observed. In figure 5*b*, a slip plane is captured below the intruder resulting in the upper block of particles moving upwards. Horizontal slip planes are also often observed (figure 5*c*).

In figure 6 the measured position of the intruder is plotted against time for a range of reduced accelerations. These plots are at a constant size ratio, $\Phi = 7$. The results in figure 6*a* correspond to the continuous regime, whereas in figure 6*b* the acceleration is lower ($\Gamma = 1.17$), and the intermittent motion is clearly visible. The results in figure 6*a* were obtained by filming at one frame per cycle; in figure 6*b* a frame was recorded every 48 cycles.

Trajectory maps of all the particles in the field were calculated for several of the experiments. Figure 7*a* shows results from one experiment with a size ratio $\Phi = 7$, and an acceleration of $\Gamma = 1.65$. This corresponds to a regime of quite strong convection; the intruder moved over the field of view in 266 frames, as indicated by its trajectory. The other trajectories all show the position of the background particles *relative to the intruder* disc. A similar plot is shown in figure 7*b*, but in this case the acceleration was reduced to $\Gamma = 1.32$ so that we are in the regime with intermittent rise characteristics. The trajectories still resemble those of figure 7*a*, showing that the intruder and background particles rise at the same average rate in a collective

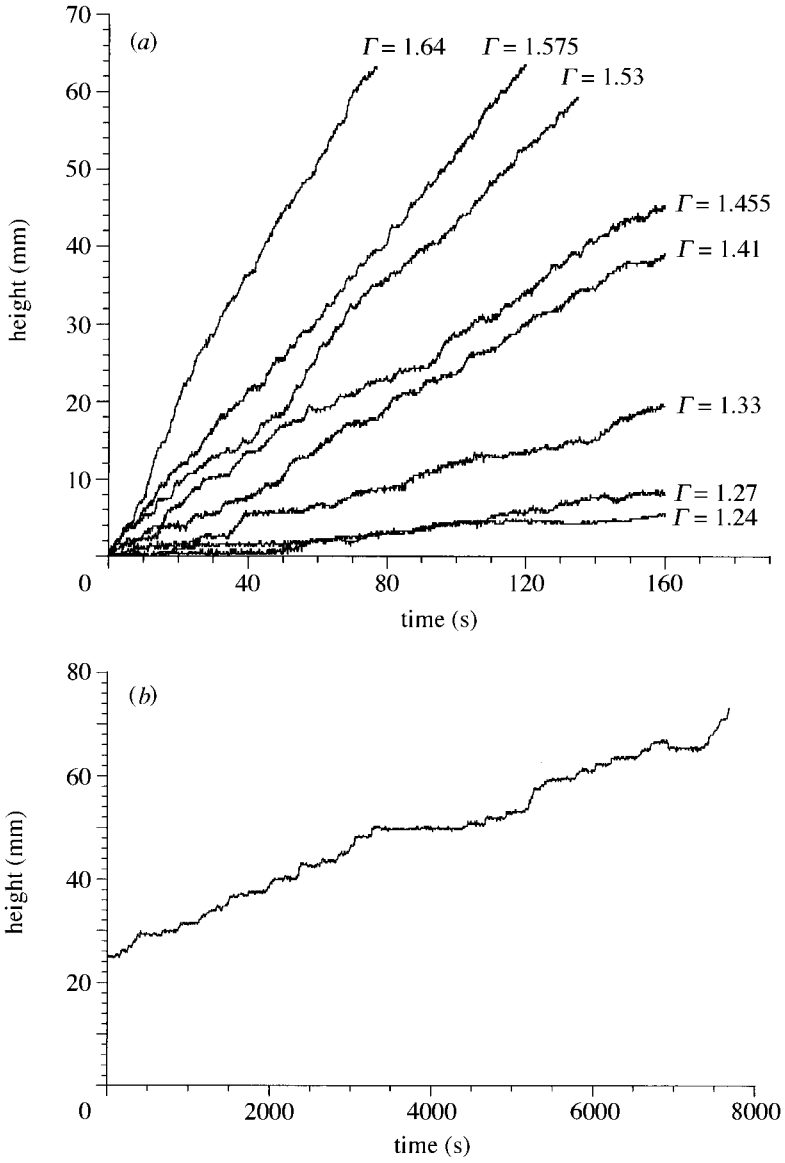

Figure 6. Intruder ascent diagrams for the (*a*) continuous and (*b*) intermittent regimes.

motion; the intruder moved over the field of view in 1355 frames. The intermittent motion of the intruder appears to be due to the relatively low frequency of slip events, each of which causes the intruder (and surrounding particles) to move upwards in a finite jump. A stable intruder appears to be present at all times, so that the slip events do not provide a driving force that pushes the intruder looking for stable positions; rather, intruder jumps are related to the height a block of particles moves during a slip event. These results and conclusions are in contrast to the concept of the intruder sampling a configuration space of stable-unstable positions as it moves upwards relative to the surrounding particles (Duran *et al*. 1993, 1994).

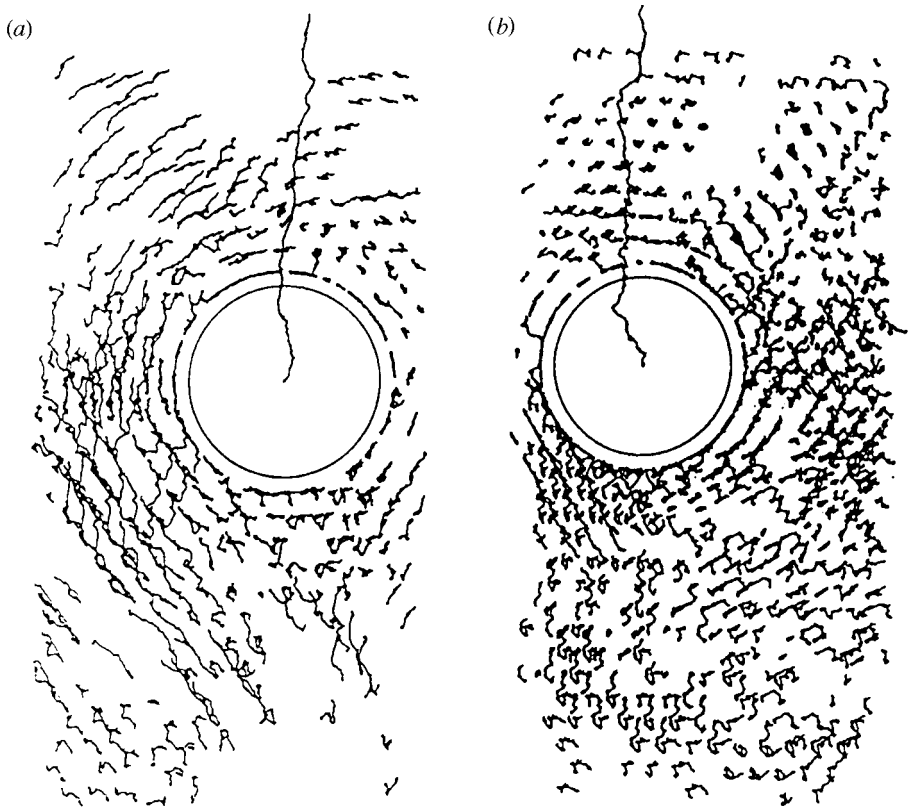

Figure 7. Trajectory maps for intruder and background particles: (*a*) $\Gamma = 1.65$; (*b*) $\Gamma = 1.32$.

4. Contact-force distribution beneath a granular pile

The transmission of stress within a granular material under quasi-static conditions is currently not well-understood. The difficulty in developing adequate theories arises for two main reasons: firstly, material nonlinearity (for example, the stiffness is zero in tension, non-zero in compression); and secondly, the lack of a unique force distribution for a given arrangement of the grains. One interesting example is the pressure distribution beneath a conical sandpile, in which, intuitively, one expects the pressure to be at a maximum at the centre. Experimental measurements have, however, shown a significant local dip at this point (Smid & Novosad 1981). This section summarizes a technique for measuring the normal contact forces exerted by the grains of a granular material on a boundary, and its application to the measurement of stress profiles beneath loosely packed conical piles (Brockbank *et al*. 1997).

The force distribution was determined by measuring the elastic deformation of a transparent silicone rubber surface on which the pile was constructed (see figure 8). The rubber layer (2.25 mm thick) was cast *in situ* on a glass flat. A hexagonal close-packed (HCP) monolayer of steel ball-bearings (2.5 mm diameter) on top of the rubber acted as a blanket of pressure sensors. The diameter of the contact region between a given ball and the rubber was measured by using an optical microscope and was related directly to the normal force acting on the ball.

The granular materials used were chosen for their variation in physical and geo-

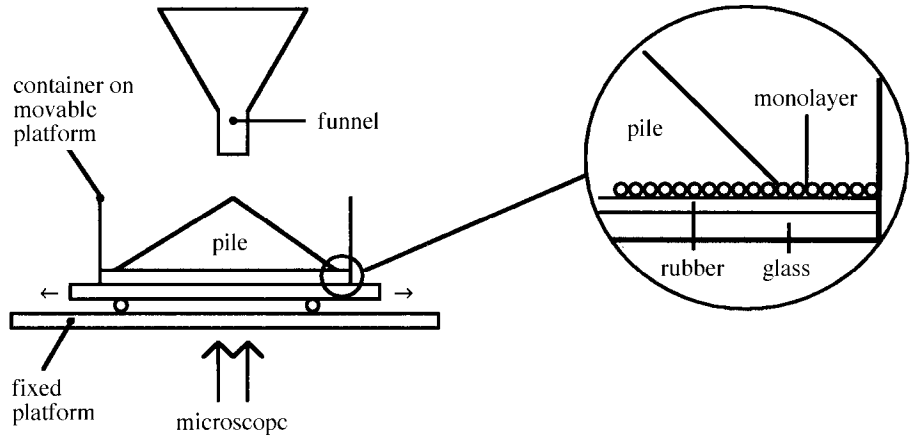

Figure 8. Experimental apparatus to measure the force profile beneath the test piles.

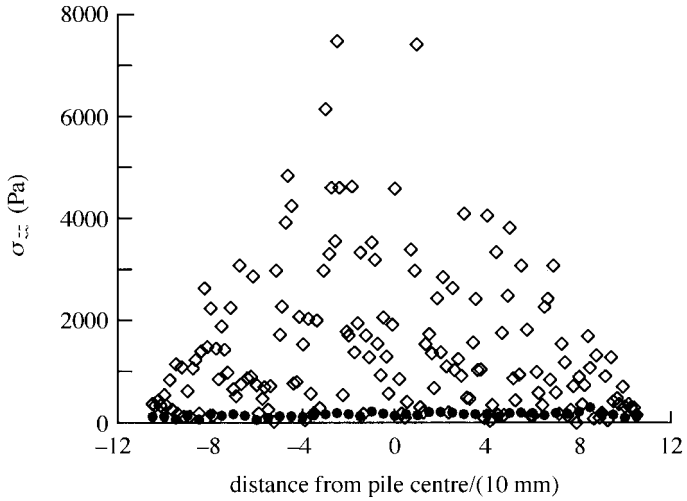

Figure 9. Pressure profiles from a lead-shot pile. Circles, ball-bearing monolayer; diamonds, lead shot.

metrical properties. Lead shot had the highest density, and the mean bead diameter was chosen to match that of the ball bearings to allow force measurements to be made on the same scale as the individual particles. Sand was used for comparison with the results of previous investigators (Smid & Novosad 1981). Two sizes of glass bead (mean diameters of 180 and 560 μm with a standard deviation of *ca.* 10%) were used to investigate the effect of particle size distribution; the effect of the friction coefficient was studied by etching the larger glass beads with a chemical etchant. Two etchant strengths increased the angle of repose by 2° and 4°, respectively. The piles were formed by pouring from a funnel at a fixed height.

The results of some of the pressure measurements made under 22 different piles of diameter *ca.* 200 mm are given in graphical form in figures 9 and 10. Figure 9 shows a typical lead-shot pile profile as measured from a single experiment. Each point represents a single contact-diameter reading. The force values show large variations

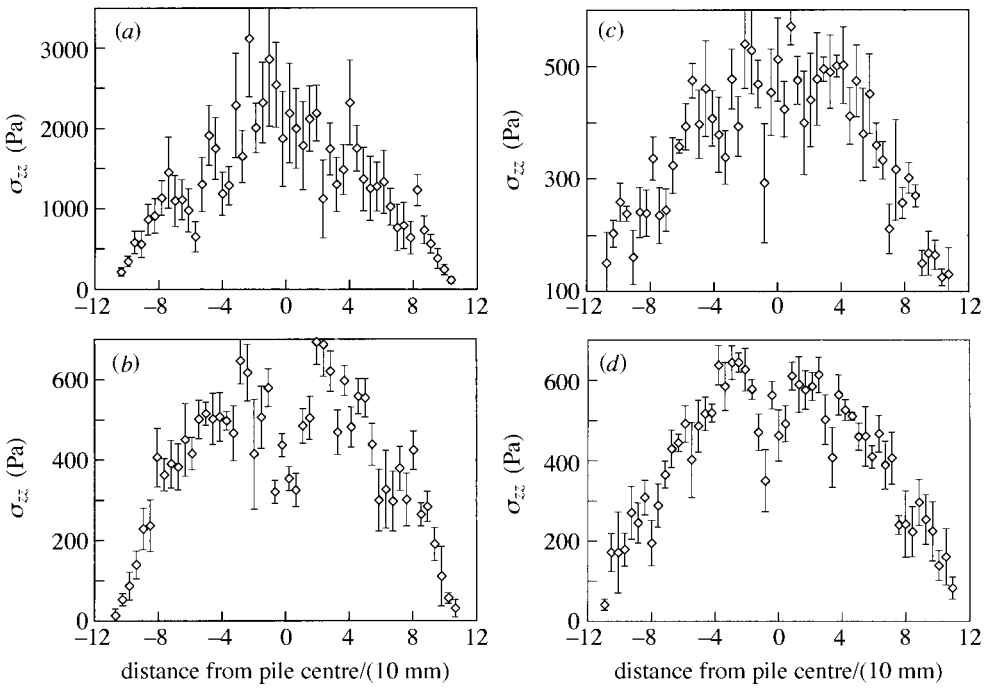

Figure 10. Pressure profiles averaged over several experiments (number of piles averaged in parentheses). (*a*) lead shot (5); (*b*) sand (3); (*c*) large glass beads (3); (*d*) small glass beads (3).

from point to point; since the diameters of the steel balls and lead grains were closely matched, this therefore represents the true fluctuations in contact forces in such a pile. The contact forces were found to follow a probability density function that was approximately negative exponential in form.

The experiment was repeated several times with each material (typically three times; five times with the lead shot), to reduce the effect of the natural contact-force fluctuations. All the results for a given material were then averaged; further averaging was also done within discrete radial ranges (bins). Some of the results are shown in figure 10, in which the error bars represent the standard deviation in the mean of the pressure values averaged. Significant pressure dips were found to occur with sand (figure 10*b*), and to a lesser extent with the small glass beads (figure 10*d*). An increase in glass-bead diameter by a factor of three resulted in almost complete suppression of the dip, regardless of whether the beads were smooth (figure 10*c*) or etched. Likewise, the much larger lead shot (figure 10*a*) showed no central minimum.

5. Microscopic models

Numerical approaches (Luding 1997; Hemmingsson *et al*. 1997) and analytical solutions (Edwards & Oakeshott 1989; Bouchaud *et al*. 1995; Edwards & Mounfield 1996; Wittmer *et al*. 1997; Bagster 1978, 1982; Liffman *et al*. 1992, 1994; Hong 1993; Huntley 1993; Opie & Grindlay 1995; Grindlay & Opie 1995) have been developed to try to explain the sandpile pressure-dip phenomenon. None has so far succeeded in

providing a completely satisfactory explanation from first principles, for the reasons mentioned in § 4.

The theoretical solutions fall into two main camps: continuum approaches (Edwards & Oakeshott 1989; Bouchaud *et al*. 1995; Edwards & Mounfield 1996; Wittmer *et al*. 1997) and microscopic models (Bagster 1978, 1982; Liffman *et al*. 1992, 1994; Hong 1993; Huntley 1993; Opie & Grindlay 1995; Grindlay & Opie 1995). Of the former, the approach by Wittmer *et al*. (1997), in which the orientation of the stress tensor is assumed to be constant at a given point in the pile throughout the process of heap formation, has proved the most successful so far in providing good agreement with experimental data. The microscopic models are somewhat simplistic, requiring, for example, the assumption of a regular lattice of grains, but, nevertheless, can be useful in giving exact analytical solutions which may provide insight into the more complicated real-life problem. The simplest of these is a pile of uniform smooth discs balanced on a rough floor on a regular diamond lattice (Bagster 1978; Liffman *et al*. 1992; Hong 1993). This may be modified by randomness in the positions of the grains in the base (Bagster 1982), vacancies in the pile (Huntley 1993), friction (Grindlay & Opie 1995) and the presence of horizontal contacts between grains (Liffman *et al*. 1994). A 'horizontal contact' between two grains refers to the situation where the grain centres and contact point are at the same height. The latter modification produced interesting results: in general terms, horizontal compressive forces generate a dip in the vertical component of force at the centre of the pile (Hemmingsson *et al*. 1997; Liffman *et al*. 1994), whereas horizontal tensile forces generate a peak (Opie & Grindlay 1995).

The two-dimensional regular-lattice model (Liffman *et al*. 1992; Hong 1993) is briefly described in § 5 *a*, followed by its extension into three dimensions (§ 5 *b*). Finally, in § 5 *c*, results from a perturbation analysis are presented that show the influence of polydispersity and small deviations from the regular lattice due to deformation of the grain contacts.

(*a*) *Two-dimensional model*

The regular-lattice model (Bagster 1978; Liffman *et al*. 1992; Hong 1993), which provides the starting point for the analysis in §§ 5 *b*, *c*, is shown in figure 11. It consists of $p-1$ layers of discs, each of diameter d; $p=10$ in this example. It is convenient to use a non-orthogonal coordinate system, (i,j), with axes along the surface diagonals. The main assumptions made are, firstly, that the contacts are frictionless; and secondly, that there are no horizontal contacts. These assumptions are necessary in order to provide a unique solution for the force field. The pile is only stable if the floor on which it is standing is rough, and thereby capable of providing a horizontal force inward to the centre of the heap. The roughness is assumed here to be due to asperities of the same spacing and diameter as the discs, which avoids the need for friction at the contacts. The bottom row of the pile (layer $p-1$) acts as this layer of asperities. The horizontal spacing of the bottom layer is chosen to be large enough to prevent horizontal contacts anywhere in the pile, i.e. the angle of repose, θ, is less than $\pi/3$. The horizontal extent of the bottom layer is $2d(p-1)\cos\theta$.

The normal forces acting along the i- and j-axes are denoted by I and J, respectively. There can be no tangential component due to the assumption of frictionless contacts. Resolving the four forces, $I(i,j)$, $I(i+1,j)$, $J(i,j)$ and $J(i,j+1)$, acting

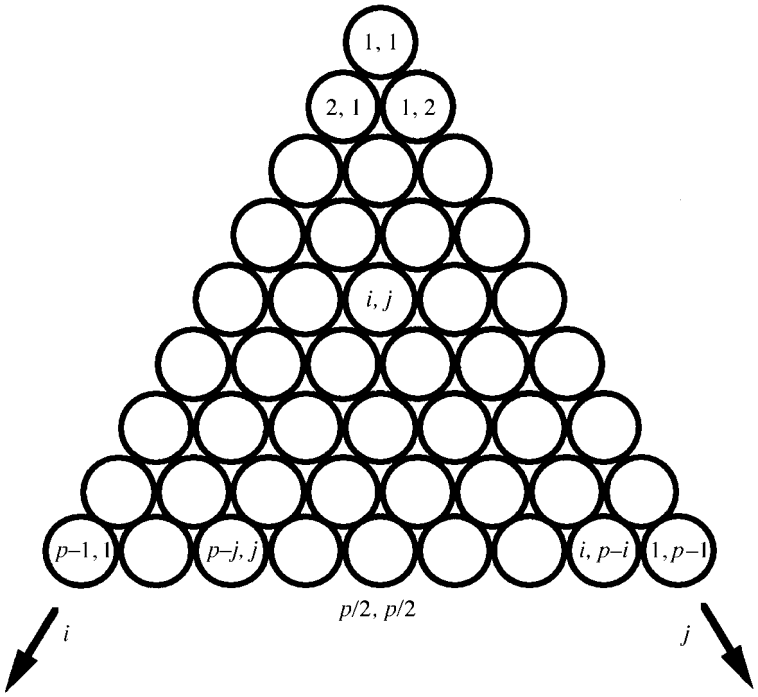

Figure 11. Model granular pile arranged on a diamond lattice. The pile consists of $p-1$ layers ($p = 10$ in this example). The support discs in the lowest layer are regarded as equivalent to the asperities on a rough floor.

on grain (i, j), both horizontally and vertically, results in two recurrence equations:

$$I(i+1, j) - I(i, j) = W/2s, \tag{5.1}$$

$$J(i, j+1) - J(i, j) = W/2s, \tag{5.2}$$

where $W = mg$ is the weight of the disc (m is the mass) and s is $\sin\theta$, where θ is the angle of repose. From equations (5.1) and (5.2), the force distribution throughout the pile is obtained as

$$I(i, j) = (i-1)W/2s, \tag{5.3}$$

$$J(i, j) = (j-1)W/2s. \tag{5.4}$$

The total vertical component of force on a disc is proportional to $(I + J)$, and since $i + j = p$ for the bottom layer, equations (5.3) and (5.4) show that the vertical component of force on the bottom layer is uniform across the pile.

(*b*) *Three-dimensional model*

Extension of the two-dimensional model in the previous section to three dimensions is straightforward for the case of a HCP ABCABC... structure. A set of three axes, i, j and k, is now required as shown in figure 12, which, as in two dimensions, follows the natural directions of contacts. $I(i, j, k)$, $J(i, j, k)$ and $K(i, j, k)$ are the contact forces acting on the particle (i, j, k) from above, along their respective axes. By choosing the angle θ between the axes and the horizontal as less than $\cos^{-1}(1/\sqrt{3})$,

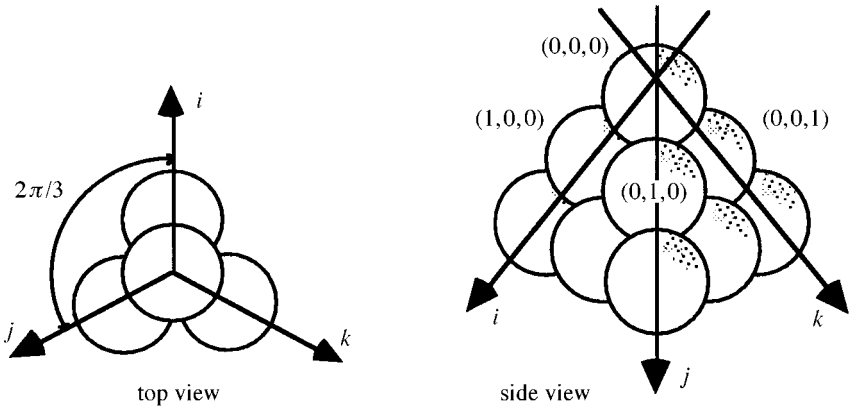

Figure 12. HCP structure (ABCABC ...) of identical spheres.

the perfectly close-packed value, there are no horizontal forces between the particles in a given layer. Each particle then experiences six contact forces, three from above and three from below. Resolving the forces vertically and horizontally once again results in recurrence relations for I, J and K, which can be solved to give

$$I(i,j,k) = (i-1)W/3s, \tag{5.5}$$

$$J(i,j,k) = (j-1)W/3s, \tag{5.6}$$

$$K(i,j,k) = (k-1)W/3s. \tag{5.7}$$

All the particles in a given layer have $i+j+k = \text{const.}$ and therefore $I+J+K$ is also constant. The vertical force component is proportional to $I+J+K$ and, as in the two-dimensional case, is therefore also constant across a given layer in the pile.

It is clear that in a real sandpile, this perfect structure and unique coordinate directions will not exist. The model can be extended relatively easily, however, by retaining the idea of the forces being transmitted at an angle to the vertical, but eliminating the preferred directions of the HCP pile. The force is therefore assumed to be transmitted uniformly through a conical shell, rather than down the three legs of the ideal HCP structure.

The new arrangement is shown in figure 13*a*. The mass element $\mathrm{d}M$ is supported by a conical shell and exerts pressure on the floor over an annular ring. The load per unit length of the ring is proportional to $\mathrm{d}M/R$, where R is the distance from $\mathrm{d}M$ to the ring. The pressure distribution could be calculated by a volume integral over the entire cone. However, an equivalent approach is to consider a single point on the base and to add up the forces due to all the mass elements that contribute to the force at that point. All such elements lie on an inverted cone (denoted cone B) as shown in figure 13*b*. The stress, σ_{ij}, at position x_0 along the diameter of the base can be written

$$\sigma_{ij}(x_0) \propto \int_{\text{area}} \frac{X_{ij}}{R}\,\mathrm{d}A, \tag{5.8}$$

where the integral is over the surface area of cone B that lies within the sandpile (cone A), R is the distance between x_0 and a point on the cone, and X_{ij} is a function to resolve the force into normal or shear stresses as required. $\mathrm{d}A$ is the small element of area containing mass $\mathrm{d}M$, lying at polar coordinates (r,ϕ). z_0 is the height of the

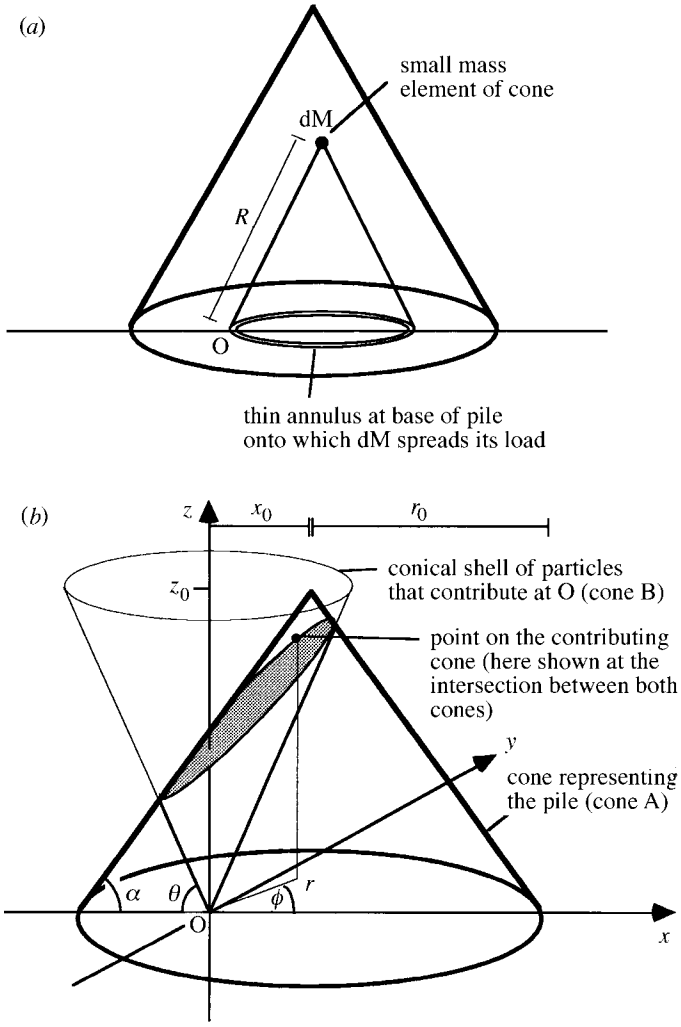

Figure 13. Model for force propagation in a randomly packed medium. (*a*) Force propagates through a conical shell rather than down the three legs of the HCP structure. (*b*) All points of cone B then contribute to the pressure at point O on the base of the pile. The symbols used are explained in the text.

cone and r_0 is its radius measured at the base. α is the angle of repose of the pile and θ (greater than α) is the angle of inclination of the contributing shell.

Equation (5.8) for the stress distribution can now be written (by using the fact that $R \propto r$ and $\mathrm{d}R \propto \mathrm{d}r$):

$$\sigma_{ij} \propto \int_{-\pi}^{\pi} \int_{0}^{r_c} X_{ij}\, \mathrm{d}R\mathrm{d}\phi = \int_{-\pi}^{\pi} X_{ij} r_c\, \mathrm{d}\phi, \tag{5.9}$$

assuming that X_{ij} is independent of R. $r_c = r_c(\phi)$ is the locus of the line of intersection of the two cones.

In the HCP structure, the force vectors pointed directly along the diagonals. Extending this to the conical-shell model, the force due to a point on the contributing

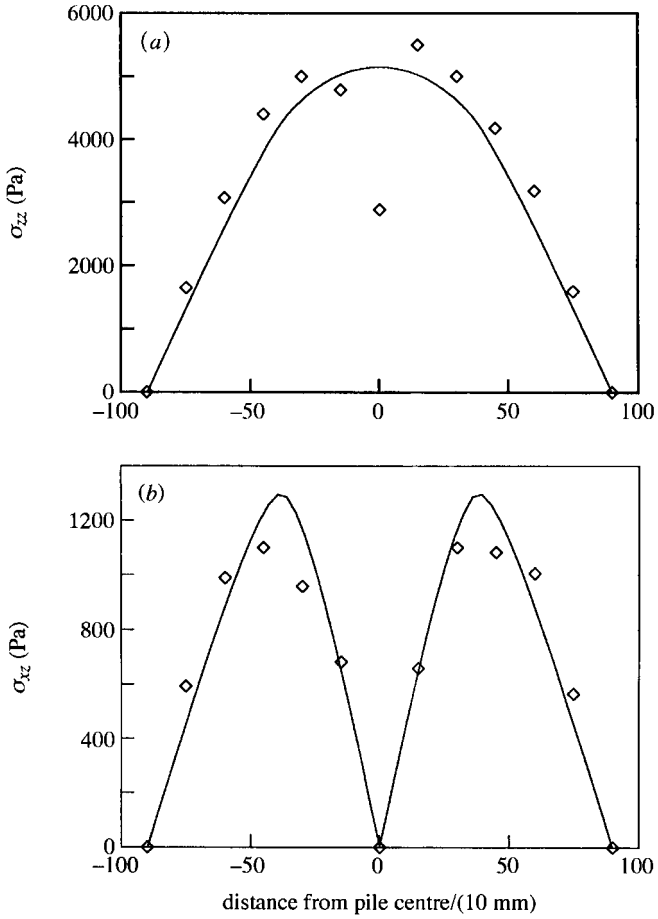

Figure 14. Fits of 'conical-shell' model stress profiles to normal and shear stress measurements obtained by Smid & Novosad (1981). (*a*) Sand, normal stress; (*b*) sand, shear stress.

cone acts along the line joining it to the vertex of the cone (the point on the base of the pile). The form of X_{ij} is, therefore,

$$X_{zz} = \sin\theta, \tag{5.10}$$

for the normal component, and

$$X_{xz} = \cos\theta\cos\phi, \tag{5.11}$$

for the shear component along the diagonal. There is no shear component perpendicular to the diagonal ($\sigma_{xy} = 0$) due to the symmetry of the problem. The equations of shear and normal stresses at the base of a conical pile can thus be written

$$\sigma_{zz} = \int_{-\pi}^{\pi} \kappa r_{\mathrm{c}} \sin\theta \,\mathrm{d}\theta, \tag{5.12}$$

$$\sigma_{xz} = \int_{-\pi}^{\pi} \kappa r_{\mathrm{c}} \cos\theta\cos\phi \,\mathrm{d}\phi, \tag{5.13}$$

where κ is a normalization constant.

It is to be expected that the lowest stress at the centre will be produced when $\theta = \alpha$, since this corresponds to the case of the weight at the centre of the pile being supported as far away from the centre as possible. The integral can then be done analytically to give the normalized stress distribution:

$$\sigma_{zz} = (1 - (x_0/r_0)^2)^{1/2}. \tag{5.14}$$

It is interesting to note that the maximum of this distribution is at $x_0 = 0$: thus, even the conditions most conducive to spreading the load to the edge of the pile fail to produce a pressure dip. Extension of the model by allowing propagation over a range of angles, rather than just a single cone angle θ, does not result in a dip either since the solution in this case is just a linear combination of the basic conical-shell solutions. The conclusion to be drawn from this analysis, therefore, is that the transmission of force in a sandpile is, in general, non-axisymmetric, presumably as a result of an anisotropic network of contacts set up during the formation of the pile.

It is, nevertheless, instructive to compare the model's predictions with experimental data. A sensitive test is to compare its predictions of the normal and shear stresses simultaneously. Equations (5.12) and (5.13) were fitted to some of the Smid & Novosad (1981) data by scaling the data for the correct κ value while varying θ, until the least-square error was obtained. Figure 14 shows the data along with the best-fit curves. The value of θ used to obtain this fit was 0.989 rad (56°), which may be compared with the value for a perfect HCP structure in which a diagonal makes an angle of 54.7° to the horizontal. For such a simple model, the functional fit appears to be quite reasonable although, as expected, the central dip in the data is not reproduced.

(*c*) *Perturbation analysis*

In this section, results from a two-dimensional analysis of the effect of small deviations from the perfect diagonal packing arrangement are summarized (Huntley 1998*b*). Two sources of irregularity are considered: (i) elastic (Hertzian) deformation of the grain–grain contacts; and (ii) systematic variations in particle size with position in the pile. The changes in stress distribution for both cases can be calculated analytically to first order in the parameter describing the perturbation.

The analysis is carried out in two steps. First, the displacement vector of each grain from its regular-lattice position (figure 11), denoted by $\boldsymbol{r}(i,j)$, is determined as a function of the disc sizes throughout the pile. Second, the equations of equilibrium for disc (i,j) can be satisfied by the superposition of forces $\delta I(i,j)$ and $\delta J(i,j)$ acting along the i- and j-axes, respectively, which are related to the first and second derivatives of $\boldsymbol{r}(i,j)$ with respect to i and j. This is illustrated in figure 15: for the distorted lattice, the forces no longer propagate independently along the i- and j-axes, as described by equations (5.1) and (5.2), but a fraction of the force along one axis can instead switch to the other axis. Integration of the forces δI and δJ from the free surfaces allows the total deviation in the vertical force component to be calculated at the base of the pile.

The result for a large sandpile ($p \to \infty$) with elastically deforming grains is

$$\delta F(\xi) = \frac{\varepsilon}{8\cos^2\theta}\{(1+\xi)^{\beta+1} + (1-\xi)^{\beta+1} - (\beta+1)[(1+\xi)(1-\xi)^{\beta} + (1-\xi)(1+\xi)^{\beta}]\}, \tag{5.15}$$

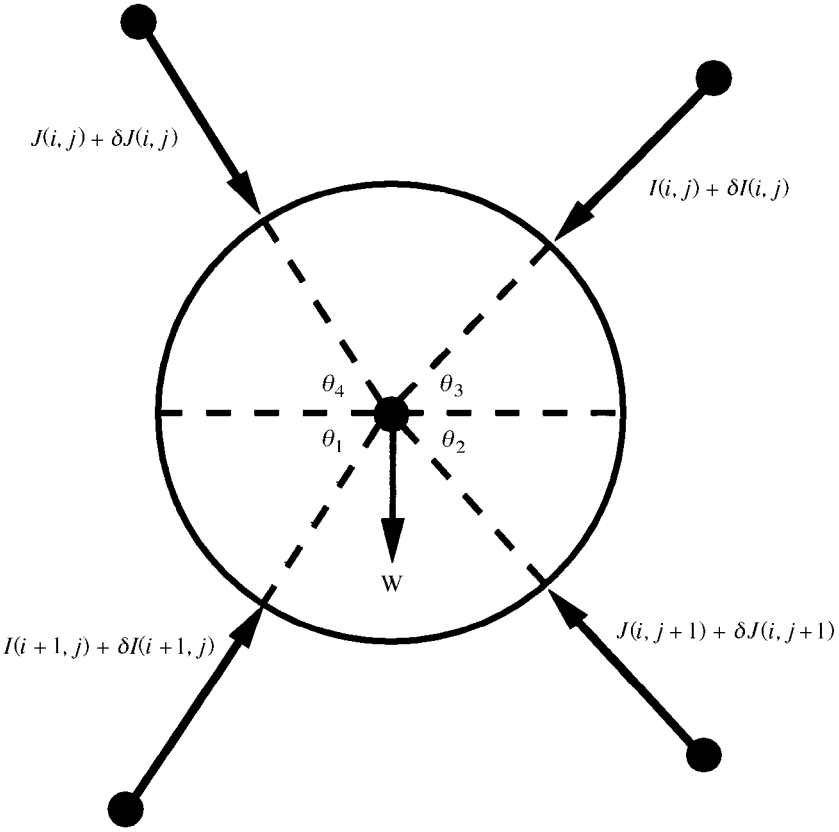

Figure 15. Forces acting on disc (i, j) in the distorted lattice. The centres of nearest neighbours are shown as •.

where $\delta F(\xi)$ is the fractional change in normal load, ξ is the normalized position along a diameter under the heap ($-1 < \xi < 1$), ε is the fractional change in diameter of the disc at the centre of the pile ($i = j = \frac{1}{2}p$) due to the deformation, and β is the exponent in the nonlinear force–displacement relationship for Hertzian contacts ($\beta = \frac{2}{3}$ for spheres). This is plotted in figure 16 for the case $\varepsilon = 0.01$, $\beta = \frac{2}{3}$, and with a horizontal separation of particle centres of $1.2d$. The results of a numerical simulation ($p = 128$) are also shown for comparison. The numerical solution involved calculating the exact displacement and force-distribution fields and shows good agreement with the first-order theoretical results. The magnitude of the pressure reduction (around 1.5% at the centre of the pile relative to the edges, for a maximum grain deformation of 1%) shows that while grain deformation might have a significant influence for low-modulus materials, it is unlikely to be the cause of the dip for most of the materials reported in experiments to date.

Variations in initial grain size are, however, a more plausible source of the necessary lattice distortions. Systematic variations in particle diameter with position in the pile can occur due to size segregation and stratification phenomena occurring during its formation (Makse *et al.* 1997). Stratification in particular can result in strong gradients in particle size in a direction normal to the free surface. A very simple

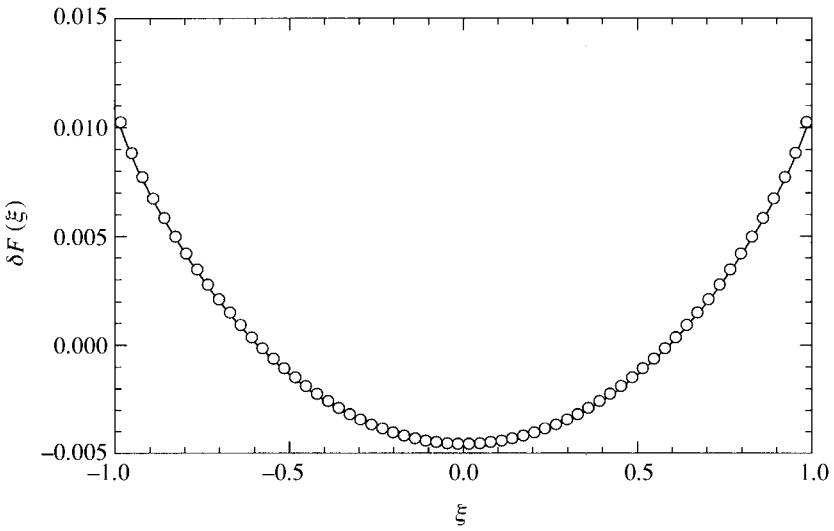

Figure 16. Non-dimensional perturbation in vertical force at base of pile due to elastic deformation at contacts ($\varepsilon = 0.01$ and $\beta = \frac{2}{3}$, corresponding to Hertzian deformation for contact between spheres). Continuous line: first-order analytical solution (equation (5.15)); discrete symbols: exact numerical solution for $p = 128$.

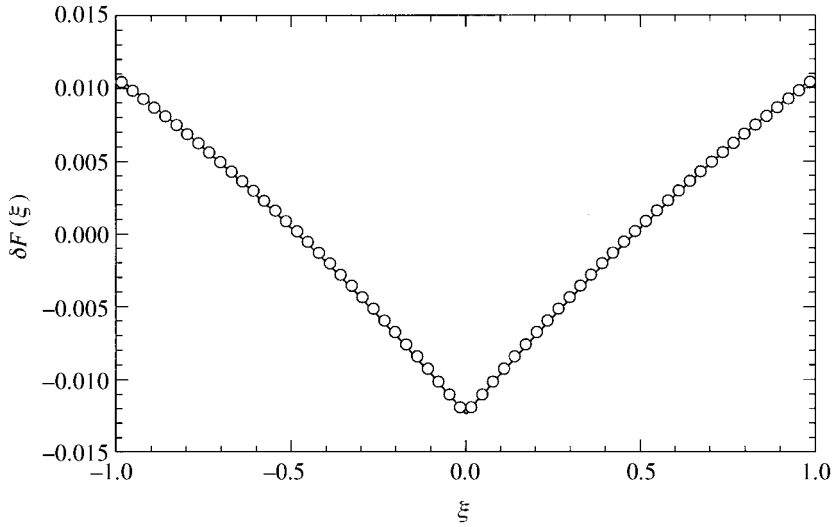

Figure 17. Non-dimensional perturbation in vertical force at base of pile due to gradient of particle sizes from the centre to the free surfaces ($\varepsilon = 0.01$). Continuous line: first-order analytical solution (equation (5.17)); discrete symbols: exact numerical solution for $p = 128$.

model of such a sandpile, in which the disc diameter, d', varies linearly with distance from the nearest free surface:

$$d'(i,j) = \begin{cases} d + a_0 i & (i < j), \\ d + a_0 j & (i \geqslant j), \end{cases} \tag{5.16}$$

results in a normalized force perturbation distribution:

$$\delta F(\xi) = \frac{\varepsilon}{4\sin^2 2\theta}[(4\cos 2\theta - 3)(1+\xi)^2 - 2(1+\cos 2\theta)(1+\xi)(1-\xi) + (1-\xi)^2] \quad (-1 < \xi \leqslant 0), \quad (5.17)$$

where $\delta F(-\xi) = \delta F(\xi)$ and $\varepsilon = pa_0/(2d)$ is the total fractional change in disc diameter between the surface and centre $(\frac{1}{2}p, \frac{1}{2}p)$ of the pile. This result was derived again for the limiting case $p \to \infty$. All piles, regardless of size (provided of course $p \to \infty$ is a good approximation), having a given fractional change in particle size from the centre to the edge will therefore have the same fractional pressure change. Figure 17 shows $\delta F(\xi)$ for the case $\varepsilon = 0.01$, i.e. the grains at the centre are 1% larger than those at the free surfaces. There is seen to be good agreement with an exact numerical solution calculated for a pile of size $p = 128$. The magnitude of the pressure dip scales in proportion to ε, and is positive (i.e. a pressure peak) for negative ε (i.e. when the small grains are at the centre). For the 1% size change considered here, the pressure dip at the centre relative to the edge is around 2.2%. The standard deviation in particle size was around 10% for the glass beads (both large and small) and over 50% for the sand grains in the experiments described in § 4. Although the model is probably too simplistic to draw firm conclusions, it seems plausible, therefore, that polydispersity can have a significant effect on the pressure profile. The details of the segregation and stratification processes occurring during the pile formation also seem likely to exert an important influence on the stress distribution.

6. Conclusions

Vibration of relatively small numbers of grains in two dimensions results in a stationary non-equilibrium state that closely approximates the equilibrium state for a gas at a uniform temperature, in which the density and speed distributions are characterized by the classical Maxwell–Boltzmann distribution. The mean particle speed is not proportional to the peak speed of the base; a simple power-balance model predicts upper and lower bound scaling exponents which are consistent with the experimentally observed values.

The main conclusion from the segregation experiments is that the intruder disc rises at the same speed as the background particles over the entire range of accelerations studied. If this phenomenon is termed convective, then the mechanism of segregation is driven by convection rolls over all accelerations. Previous studies which indicate that convection is absent at low accelerations (i.e. upwards motion of the intruder is not accompanied by upwards motion of the surrounding particles) and that geometrical effects strongly influence the segregation mechanism, are not supported by these observations.

The experimental measurements of force distribution under a sandpile have confirmed the existence of a counter-intuitive pressure dip at the centre of the pile, at least for some of the granular materials tested. The magnitude of the dip was largest for piles made of sand; for glass spheres it appeared to be dependent on particle size distribution but not on the grain–grain friction coefficient. The main conclusions to be drawn from the microscopic models described in the paper are, first, that the transmission of force in a sandpile is in general non-axisymmetric, and, second, that

local changes in packing geometry caused by segregation and stratification can be expected to exert a significant influence on the stress distribution.

The research summarized in this paper benefited from experimental and theoretical input from S. Warr, R. Brockbank, R. C. Ball, W. Cooke, G. T. H. Jacques and H. T. Goldrein; technical support from D. Johnson, R. Flaxmann and P. Bone; and useful discussions with C. C. Mounfield, S. F. Edwards, J. E. Field and E. M. Terentjev. The model described in § 5 *b* was developed during discussions with R. C. Ball and R. Brockbank, and figure 14 was prepared by R. Brockbank. Funding from the Department of Trade and Industry, the EPSRC, Unilever Plc, ICI Plc, Zeneca Plc, Schlumberger Cambridge Research and Shell International Oil Products is also gratefully acknowledged.

References

Bagster, D. F. 1978 An idealised model of granular material behaviour in ore heaps and hoppers. *J. Powder Bulk Solids Technol.* **2**, 42.

Bagster D. F. 1982 A randomised model of granular material behaviour in an ore heap. *J. Powder Bulk Solids Technol.* **6**, 1.

Bouchaud, J.-P., Cates, M. E. & Claudin, P. 1995 Stress distribution in granular media and nonlinear wave equation. *J. Phys. France* I **5**, 639.

Brockbank, R., Huntley, J. M. & Ball, R. C. 1997 Contact force distribution beneath a three-dimensional granular pile. *J. Phys. France* II **7**, 1521.

Campbell, C. S. 1990 Rapid granular flows. *A. Rev. Fluid Mech.* **22**, 57.

Clement, E. & Rajchenbach, J. 1991 Fluidization of a bidimensional powder. *EuroPhys. Lett.* **16**, 133.

Cooke, W., Warr, S., Huntley, J. M. & Ball, R. C. 1996 Particle size segregation in a two-dimensional bed undergoing vertical vibration. *Phys. Rev.* E **53**, 2812.

Douady, S., Fauve, S. & Laroche, C. 1989 Subharmonic instabilities and defects in a granular layer under vertical vibrations. *Europhys. Lett.* **8**, 621.

Duran, J., Rajchenbach, J. & Clement, E. 1993 Arching effect model for particle-size segregation. *Phys. Rev. Lett.* **70**, 2431.

Duran, J., Mazozi, T., Clement, E. & Rajchenbach, J. 1994 Size segregation in a 2-dimensional sandpile—convection and arching effects. *Phys. Rev.* E **50**, 5138.

Edwards, S. F. & Mounfield, C. C. 1996 A theoretical model for the stress distribution in granular matter. III. Forces in sandpiles. *Physica* A **226**, 25.

Edwards, S. F. & Oakeshott, R. B. S. 1989 The transmission of stress in an aggregate. *Physica* D **38**, 88.

Evesque, P. 1992 Shaking dry powders and grains. *Contemp. Phys.* **33**, 245.

Evesque, P. & Rajchenbach, J. 1989 Instability in a sand heap. *Phys. Rev. Lett.* **62**, 44.

Grindlay, J. & Opie, A. H. 1995 Contact force distribution in a pile of rigid disks. *Phys. Rev.* E **55**, 718.

Helal, K., Biben, T. & Hansen, J. P. 1997 Local fluctuations in a fluidized granular medium. *Physica* A **240**, 361.

Hemmingsson, J., Herrman, H. J. & Roux, S. 1997 Vectorial cellular automaton for the stress in granular media. *J. Phys. France* I **7**, 291.

Hong, D. C. 1993 Stress distribution of a hexagonally packed granular pile. *Phys. Rev.* E **47**, 760.

Huntley, J. M. 1993 Vacancy effects on the force distribution in a two-dimensional granular pile. *Phys. Rev.* E **48**, 4099.

Huntley, J. M. 1998*a* Scaling laws for a two-dimensional vibro-fluidized granular material. *Phys. Rev.* E. (In the press.)

Huntley, J. M. 1998*b* Force distribution in an inhomogeneous sandpile. *Eur. Phys. Rev.* B. (In the press.)

Jaeger, H. M. & Nagel, S. R. 1992 Physics of the granular state. *Science* **255**, 1523.

Knight, J. B., Jaeger, H. M. & Nagel, S. R. 1993 Vibration-induced size separation in granular media—the convection connection. *Phys. Rev. Lett.* **70**, 3728.
Liffman, K., Chan, D. Y. C. & Hughes, B. D. 1992 Force distribution in a two dimensional sandpile. *Powder Technol.* **72**, 255.
Liffman, K., Chan, D. Y. C. & Hughes, B. D. 1994 On the stress depression under a sandpile. *Powder Technol.* **78**, 263.
Luding, S. 1997 Stress distribution in static two-dimensional granular model media in the absence of friction. *Phys. Rev.* E **55**, 4720.
Luding, S., Clement, E., Blumen, A., Rajchenbach, J. & Duran, J. 1994*a* Studies of columns of beads under external vibrations. *Phys. Rev.* E **49**, 1634.
Luding, S., Herrmann, H. J. & Blumen, A. 1994*b* Simulations of two-dimensional arrays of beads under external vibrations: scaling behaviour. *Phys. Rev.* E **50**, 3100.
Makse, H. A., Havlin, S., King, P. R. & Stanley, H. E. 1997 Spontaneous stratification in granular mixtures. *Nature* **386**, 379.
Opie, A. H. & Grindlay, J. 1995 Deformation of an elastic triangle in equilibrium under gravity. *Phys. Rev.* E **55**, 724.
Pak, H. K. & Behringer, R. P. 1993 Surface-waves in vertically vibrated granular-materials. *Phys. Rev. Lett.* **71**, 1832.
Savage, S. B. 1984 The mechanics of rapid granular flows. *Adv. Appl. Mech.* **24**, 289.
Smid, J. & Novosad, J. 1981 Pressure distribution under heaped bulk solids. *IChemE Symp.* **63**, D3/V/1.
Warr, S. & Huntley, J. M. 1995 Energy input and scaling laws for a single particle vibrating in one-dimension. *Phys. Rev.* E **52**, 5596.
Warr, S., Jacques, G. T. H. & Huntley, J. M. 1994 Tracking the translational and rotational motion of granular particles: use of high speed photography and image processing. *Powder Technol.* **81**, 41.
Warr, S., Huntley, J. M. & Jacques, G. T. H. 1995 Fluidisation of a two-dimensional granular system: experimental study and scaling behaviour. *Phys. Rev.* E **52**, 5583.
Warr, S., Cooke, W., Ball, R. C. & Huntley, J. M. 1996 Probability distribution functions for a single-particle vibrating in one dimension: experimental study and theoretical analysis. *Physica* A **231**, 551.
Wittmer, J. P., Cates, M. E. & Claudin, P. 1997 Stress propagation and arching in static sandpiles. *J. Phys. France* I **7**, 39.